Total cross sections and thermonuclear reaction rates for $^9Be(\alpha,n)^{12}C$

P. R. Wrean, C. R. Brune, and R. W. Kavanagh
W. K. Kellogg Radiation Laboratory, 106-38, California Institute of Technology, Pasadena, California 91125
(Received 30 August 1993)

The $^9Be(\alpha,n)^{12}C$ reaction determines the rate for neutron-catalyzed helium burning and thus plays an important role in supernovae ejecta under α- and n-rich conditions which may lead to the r process. Cross sections for this reaction have been measured for $0.16 \leq E_{c.m.} \leq 1.87$ MeV using a 4π neutron detector, and are used to calculate the thermonuclear reaction rates for temperatures between 0.1 and 10 GK. During these measurements, the thick-target yields were determined for $0.50 \leq E_\alpha \leq 2.30$ MeV, the stopping powers for α's in beryllium determined for $0.24 \leq E_\alpha \leq 2.12$ MeV, and the $^9Be(p,p)$ elastic scattering cross sections measured at $\theta_{lab} = 142.4°$ for $2.34 \leq E_p \leq 2.66$ MeV.

PACS number(s): 25.55.Hp, 95.30.Cq, 27.20.+n

I. INTRODUCTION

The nucleosynthesis of ^{12}C in first-generation stars is commonly ascribed to the "triple-alpha" reaction, $3\alpha \rightarrow {}^{12}C + \gamma$. This reaction follows hydrogen burning in the red-giant stage, occurring as the core contracts and heats to densities $\rho \approx 10^5$ g/cm^3 and temperatures $T \approx 10^8$ K. Proceeding through a resonant state [1] in ^{12}C at 7.65 MeV, this reaction bypasses the unstable nuclei at $A = 5$ and 8 that inhibit a more rapid sequence of two-body reactions leading to ^{12}C.

In n- and α-rich regions of supernovae ejecta, however, the reaction $^4He + n + {}^4He \rightarrow {}^9Be + \gamma$ is by far the most dominant bridge, as explored in reaction-network calculations [2] by Delano and Cameron. Recently, Woosley and Hoffman [3] corroborated this finding when extending such supernova calculations to include the nucleosynthetic effects of the large flux of high-energy neutrinos from the nascent neutron star. They suggest that a neutrino-induced "wind" may provide the long-sought mechanism for ejection of processed material into the interstellar medium. They also find that charged particle reactions are important for initiating the r process and in fact the classical r process may not start from iron but rather from nuclei of mass ≈ 100 produced by α particle reactions.

These reactions are initiated by neutron-catalyzed helium burning, $^4He(\alpha n,\gamma)^9Be(\alpha,n)^{12}C$, which occurs 40 times faster than the triple-alpha reaction for $T \approx 4$ GK, $\rho \approx 5 \times 10^4$ g/cm^3. Under these conditions, the reaction $2\alpha + n \leftrightarrow {}^9Be^*$ is near equilibrium, involving mainly the broad first excited state of ^9Be at 1.68 MeV. The equilibrium abundance of the $^9Be^*$ can be calculated for the ambient conditions by a shape-weighted integral over the (asymmetric) level profile [4]. Then the leakage to $^9Be(gnd)$ is determined by the known $E1$ width [5], $\Gamma_{\gamma 1} = 0.30 \pm 0.12$ eV, with E_γ^3 weighting.

The ^9Be thus formed is then burned to ^{12}C by the $^9Be(\alpha,n)^{12}C$ reaction ($Q = 5.70$ MeV), in competition with other destruction reactions, including $^9Be(\gamma,n)$, (n,γ), (n,α), and $(n,2n)$, with (γ,n) dominant. Previous total-cross-section measurements of the (α,n) reaction, for $0.24 \leq E_{c.m.} \leq 0.47$ MeV [6], $1.0 \leq E_{c.m.} \leq 5.4$ MeV [7], and $1.2 \leq E_{c.m.} \leq 7.3$ MeV [8], lead to reaction rates [9] with an estimated error [10] of a factor of 3 in the temperature range 2–5 GK. This error was identified by Woosley and Hoffman [3] as the largest in determining the production of ^{12}C; here we report measurements of the $^9Be(\alpha,n)^{12}C$ cross sections which, taken with the earlier cited work, establish the reaction rates to a precision of $\pm 10\%$ for $0.1 \leq T \leq 10$ GK (Sec. III C below). Above $T = 0.2$ GK, our rates differ by up to $\approx 65\%$ compared with those of Ref. [9], and are a factor of 7 higher near $T = 0.15$ GK.

During target-thickness measurements, we found the stopping powers for α's in beryllium (Sec. II C) to be $\approx 15\%$ higher than those given by Ziegler [11] for $0.24 \leq E_\alpha \leq 2.12$ MeV. We also measured the thick-target yields for $0.50 \leq E_\alpha \leq 2.30$ MeV (Sec. II D), which agree with the numerical integration of our measured cross sections when combined with our stopping powers. For bombarding energies of 1.60 and 1.80 MeV, our thick-target yields are considerably higher than the yields recently reported by Heaton *et al.* [12], but the yields agree very well for the energy range $2.00 \leq E_\alpha \leq 2.30$ MeV.

II. EXPERIMENTAL METHOD

The 3-MV Pelletron tandem accelerator at the Kellogg Radiation Laboratory provided the proton and $^4He^+$ beams used in this experiment. Beam energy was determined by a 90° magnetic analyzer whose field was measured by a NMR gaussmeter. The energy calibration was verified ($\pm 0.1\%$) using the 2574.2 ± 0.7-keV neutron threshold [13] in $^{18}O(p,n)^{18}F$, and the 1928.4 ± 0.6-keV resonance [14] in $^{18}O(p,\gamma)^{19}F$, and was consistent with previous calibrations using the 991.86 ± 0.03-keV resonance [15] in $^{27}Al(p,\gamma)^{28}Si$, the 606.0 ± 0.5-keV resonance [16] in $^{11}B(\alpha,n)^{14}N$, and the 1530.03 ± 0.15-keV reso-

nance [17] in ^{24}Mg$(\alpha,\gamma)^{28}$Si. The energy resolution of the beam, < 0.5 keV, was less than the 1.5-keV width of our thinnest target. Beam-line and target vacuums were maintained at $< 7 \times 10^{-7}$ Torr. Beam currents were varied between 3 nA and 30 μA to achieve the desired count rate. The beam spot was defined by a 1.25-cm-diam collimator 60 cm upstream from the target, and a -400-V suppression ring between the target and collimator ensured accurate current integration. To minimize target deterioration, the focused beam was swept through an area of ≈ 1 cm^2 on each target, and targets were freon-cooled for beam currents above 1 μA.

A. Neutron detection

The neutron yields were measured using a 4π detector [18] consisting of 11 thermal-neutron detectors (^{3}He-filled proportional counters) embedded in a polyethylene-cube moderator surrounding the target chamber.

Because the efficiency of the detector is dependent on neutron energy, we used Monte Carlo calculations to find the efficiencies for the neutron-energy distributions expected. For our experimental α-particle energies, the ^{9}Be$(\alpha,n)^{12}$C reaction populates both the first excited state and the ground state of ^{12}C, with associated neutrons n_1 and n_0. The ratio of n_1 to n_0 neutrons, and consequently the detection efficiency, is a function of the bombarding alpha-particle energy. For $1.0 \leq E_{\text{c.m.}} \leq 2.1$ MeV, this ratio was taken from the tabulation by Geiger and Van der Zwan [19]. Below 1 MeV, the ratio was taken to be 1:1, consistent with the values derived from Davids [6] for $0.34 \leq E_{\text{c.m.}} \leq 0.43$ MeV.

The Monte Carlo calculations were checked by measuring the detector efficiency for the following: the efficiency was $(20.3 \pm 0.6)\%$ for a ^{252}Cf source ($\bar{E}_n = 2.35$ MeV) whose strength is known to within 3%; the efficiency was $(15.6 \pm 0.3)\%$ for a 10-mCi ^{241}Am-Be source ($\bar{E}_n = 4.46$ MeV) whose strength was determined by comparison with a 1-Ci AmBe source which had been calibrated recently by NIST to within 1.7%; and the efficiency was $(7.7 \pm 0.2)\%$ at $\bar{E}_n = 14.1$ MeV, determined using the ^{3}H$(d,n)^4$He reaction. The Monte Carlo values for the ratios of the AmBe/^{252}Cf and ^{3}H$(d,n)^4$He/^{252}Cf efficiencies were 0.789 ± 0.011 and 0.386 ± 0.004, agreeing well with the measured ratios of 0.77 ± 0.03 and 0.382 ± 0.011, respectively. Based on the observed agreement, the Monte Carlo calculations, normalized to the measured source strengths, were used for calculating the efficiency.

Including the uncertainties in the source strengths, the Monte Carlo calculations, and the n_1 to n_0 ratio, the error in the efficiency is estimated to be 8%.

B. Target-thickness determination

Five targets of thicknesses varying between 0.76 and 131 μg/cm^2 were made by evaporating pure beryllium onto etched copper disks. A blank copper disk was also prepared to verify that the neutron background from alpha bombardment of any impurities in the copper substrate was negligible. In addition, this copper blank proved useful as a calibration standard in the elastic-scattering work described below.

The ^{9}Be areal densities of the three thickest targets were determined to within 3% using both elastic proton scattering and proton energy loss. The scattered protons were detected at $\theta_{\text{lab}} = 142.4°$ with a silicon surface-barrier detector collimated to have a solid angle of 1.18 ± 0.02 msr. The energy calibration of the detector was established using the leading edges of the plateaus resulting from the scattering of variable-energy proton beams from thick beryllium, aluminum, and copper substrates.

A 1.0-mm thick Be disk was bombarded with protons using the same detection setup to determine $\frac{d\sigma}{d\Omega}(\theta_{\text{lab}} = 142.4°)$ for ^{9}Be(p,p) around $E_p \approx 2.5$ MeV, where the cross section is greatly enhanced relative to the Rutherford value. A correction of $\approx 3\%$ was made to the spectrum to correct for the background of deuterons and alpha particles produced by other ^{9}Be $+ p$ reactions. Figure 1 shows a typical spectrum. The formalism of Bardin

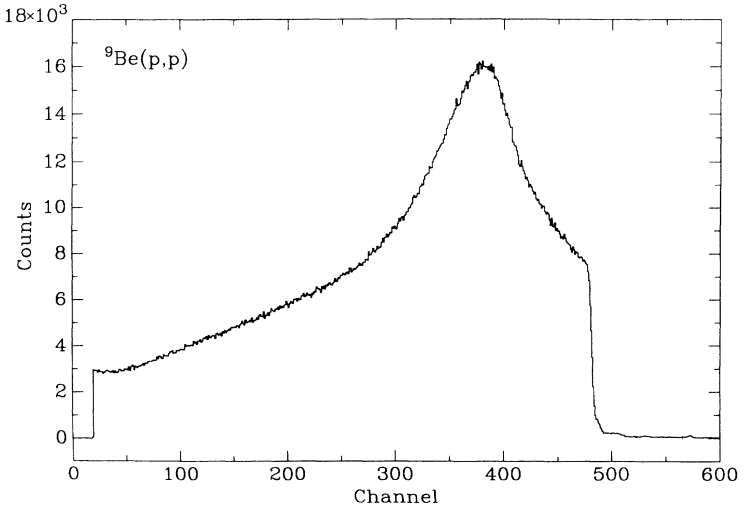

FIG. 1. Typical spectrum for ^{9}Be(p,p) scattering measurements using a thick ^{9}Be disk for incident $E_p = 2.675$ MeV. The incident charge was 17.20 μC.

[20] was used to analyze the spectrum of particles scattered by a thick target. The technique was tested by bombarding a Cu substrate with 2.5-MeV protons, where the cross section is known to be governed by the Rutherford law [21]. Using Ziegler's stopping powers [11], we found the measured cross sections for $Cu(p,p)$ to be within 3% of the Rutherford formula for proton energies ranging from the bombarding energy down to 300 keV below the bombarding energy. Ziegler's fit to the stopping powers in the required range ($1.6 \leq E_p \leq 2.6$ MeV) is primarily based upon the measurements of Andersen *et al.* [22], which quote a 0.3% uncertainty. The thick beryllium disk was then bombarded with ten incident proton energies varying between 2.475 and 2.675 MeV. The inferred $d\sigma/d\sigma_R$ for $2.30 \leq E_p \leq 2.65$ MeV for all runs agreed within 2%, with a typical result shown in Fig. 2. We find the resulting $(d\sigma/d\sigma_R)_{\max}$ at $E_p = 2.522 \pm 0.004$ MeV to be 39.5 ± 1.2, where the uncertainty includes contributions from beam-current integration, solid angle, stopping powers, detector energy calibration, detector angle, and background corrections. Our values for both the $(d\sigma/d\sigma_R)_{\max}$ and the energy of this maximum agree with the values given by Mozer [23] and Kiss *et al.* [24], but disagree with the values given by Langley *et al.* [25].

The $^9Be(p,p)$ measurements were then repeated with the three thickest copper-backed targets, with a typical spectrum shown in Fig. 3. As shown in the figure, the proton peak does not overlap the small peaks due to other $^9Be + p$ reaction products. It should be noted that the great enhancement of the $^9Be(p,p)$ cross section relative to the Rutherford formula makes it possible to measure easily the elastic-scattering yield from ^9Be deposits on relatively high-Z substrates. Both the shift in the leading edge of the copper scattering plateau, due to the layer of Be on the surface, and the area of the beryllium scattering peak were measured, giving independent determinations of the Be layer thickness, using our $d\sigma/d\Omega$. The two methods are not completely independent, as they both use the stopping power of protons in beryllium, but the uncertainty in the stopping power makes a negligible contribution to the total uncertainty in the thickness determined by either method. These two methods gave consistent results, with an areal density of $(1.23 \pm 0.04) \times 10^{18}$ atoms/cm^2 (18.4 μg/cm^2) of ^9Be for the target used to determine (α,n) cross sections over the entire energy range.

The thicknesses of the two thinnest targets, 0.76 and 2.79 μg/cm^2, were determined by comparing their $^9Be(\alpha,n)^{12}C$ nonresonant yields with the yield of the 18.4-μg/cm^2 target.

C. Stopping powers of α's in beryllium

We measured the stopping powers of α's in beryllium for $0.24 \leq E_\alpha \leq 2.12$ MeV by examining the shift in the leading edge of the copper scattering plateau in the copper-backed Be targets for incident α particles between 0.40 and 2.50 MeV. The measurements were performed with the 48.3- and 131-μg/cm^2 targets using the same setup as for the proton scattering work described above. When the 131-μg/cm^2 target was bombarded with a 0.60-MeV α-particle beam, the elastic scattering from the underlying copper was completely stopped in the target. Under these circumstances, the $A > 9$ contaminants in the Be layer could be determined by Rutherford backscattering. The dominant contaminants were found to be 0.3% of $A \approx 28$ uniformly distributed in the beryllium, and a 1.7×10^{16}-atoms/cm^2 surface layer of oxygen. Figure 4 shows the results for the stopping powers, including both Ziegler's formula [11] and the fit to our data, and also includes the experimental results from other authors [26,27]. The empirical fit to our results, used for all subsequent data analysis, has the form

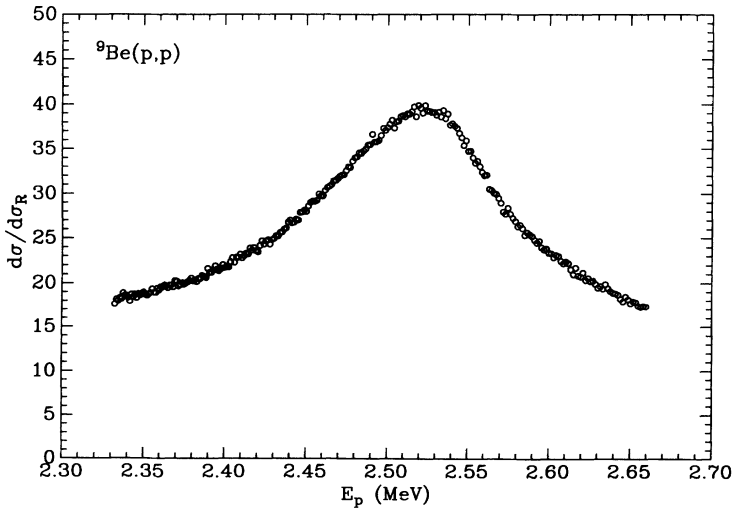

FIG. 2. $^9Be(p,p)$ elastic-scattering cross sections, inferred from the spectrum in Fig. 1, measured at $\theta_{\rm lab} = 142.4°$ for incident $E_p = 2.675$ MeV.

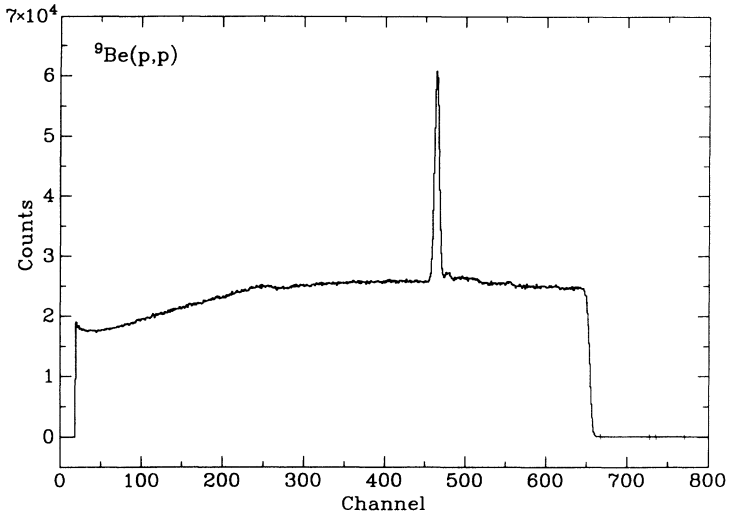

FIG. 3. Typical spectrum for ^{9}Be(p,p) thin-target scattering measurements using the 48.3-μg/cm^2 ^{9}Be target at E_p = 2.525 MeV, with incident charge 73.40 μC. The narrow peak at channel 460 is the ^{9}Be(p,p) scattering peak. The underlying plateau is due to Cu(p,p) scattering.

$$\left(\frac{dE}{dX}\right)_{\text{ours}} = \left(\frac{dE}{dX}\right)_{\text{Ziegler}} \left[1.0412 + 7.167 \times 10^{-4} E_\alpha \exp\left(\frac{-E_\alpha}{510.7}\right)\right] , \quad (1)$$

where Ziegler's expression is

$$\left(\frac{dE}{dX}\right)_{\text{Ziegler}} = \frac{S_{\text{low}} S_{\text{high}}}{S_{\text{low}} + S_{\text{high}}} , \quad (2)$$

where S_{low} and S_{high} are given by

$$S_{\text{low}} = 2.206 E_\alpha^{0.51} \quad (3)$$

and

$$S_{\text{high}} = \frac{1.532 \times 10^4}{E_\alpha} \ln\left(1 + \frac{250}{E_\alpha} + 0.008\,995 E_\alpha\right) , \quad (4)$$

respectively. E_α is measured in keV, and the dimension of the stopping power dE/dX is eV/(10^{15} atoms/cm^2), consistent with Ziegler's notation. Our expression is valid only over the range of our data, $0.24 \leq E_\alpha \leq 2.12$ MeV.

Our results, with an uncertainty of 3%, are up to 17% higher than those in Ziegler's tabulation; this has significant effects upon the analysis described below. In particular, the use of Ziegler's dE/dX and the Be thicknesses for the 18.4- and 48.3-μg/cm^2 targets determined as described above lead to discrepancies between deduced and observed widths of the narrow ^{9}Be$(\alpha,n)^{12}$C resonance at $E_{\text{c.m.}} = 0.428$ MeV.

D. Yield measurements

The neutron yields were measured for $0.16 \leq E_{\text{c.m.}} \leq 1.87$ MeV using the 18.4-μg/cm^2 ^{9}Be target. The yields

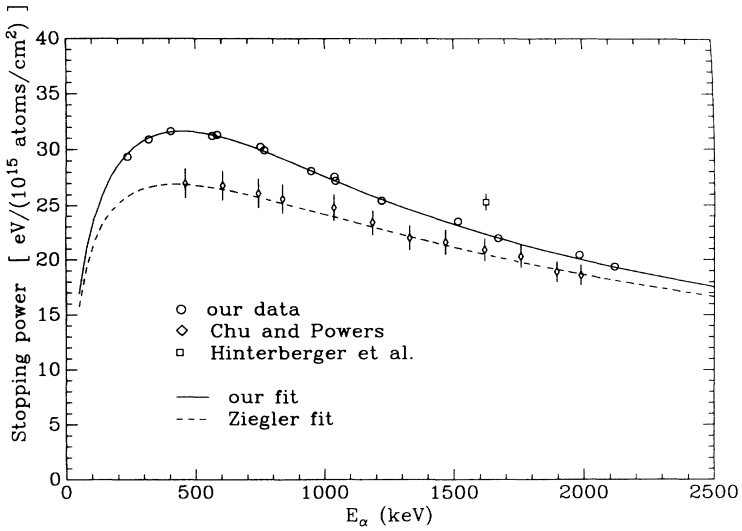

FIG. 4. Measured stopping powers for α particles in beryllium using two ^{9}Be targets of thicknesses 48.3 and 131 μg/cm^2. Our data points have uncertainty of 3%.

were first corrected for the dead time of the detector; this correction was less than 0.5% for all points. The background subtraction was less than 0.2% for the yields with $E_{\text{c.m.}} > 0.29$ MeV. The rapid drop in the cross section below 0.29 MeV required larger beam currents which damaged the target, but as these measurements were the last to be taken, only the lowest-energy data points were affected. The yields were corrected for this effect, assuming that the loss in target thickness was linear with the accumulated charge. The correction was less than 1% for yields with $E_{\text{c.m.}} > 0.32$ MeV, and less than 5% for yields with $E_{\text{c.m.}} > 0.25$ MeV.

The narrow resonance at $E_{\text{c.m.}} = 0.428$ MeV was examined in more detail using two thinner ^{9}Be targets of areal densities 2.79 and 0.76 μg/cm^2, and one thick target of areal density 48.3 μg/cm^2. These yields had dead time and background corrections similar to those described above.

As a check on our target-thickness measurements, the thick-target neutron yields were measured for $0.50 \leq E_\alpha \leq 2.30$ MeV using the same thick Be disk used for the ^{9}Be(p,p) scattering work. The dead time correction was $< 1\%$ for yields below 1.80 MeV, and the background correction was negligible.

As a further check of the target thickness and neutron detection efficiency, the ^{9}Be(p,n) yield for the peak of the resonance at 2.56 MeV was measured using the 48.3-μg/cm^2 target. The yield was corrected by 13% for the Cu(p,n) contribution from the substrate of the target, found by bombarding the blank copper disk. Using 0.203 ± 0.006 for the value of the efficiency, we find a value of 158 ± 7 mb for the ^{9}Be(p,n) cross section, agreeing well with the value of 160 mb given by Gibbons and Macklin [28].

III. RESULTS

A. Calculation of cross sections

The yield of neutrons detected per incident particle, Y_n, for an ideal target and monoenergetic beam of energy E, is given by

$$Y_n = (nt)\sigma(E)\varepsilon(E) , \tag{5}$$

where (nt) is the areal number density of target atoms, σ is the reaction cross section, and ε is the neutron-detection efficiency. For a target which is not infinitesimally thin, the beam loses energy as it passes through the target, and the yield is then given by

$$Y_n = \int_{E_t}^{E} \sigma(E')\varepsilon(E') \left[\frac{dE}{dX}(E')\right]^{-1} dE' , \tag{6}$$

in which $E_t = E - \Delta E$, where ΔE is the energy loss of the beam in the target, E is the bombarding alpha-particle energy, and $\frac{dE}{dX}(E')$ is the stopping power of α's in beryllium. Here the laminar thickness dX in the stopping power is measured in target atoms per unit area. Thus, the average energy of the beam in the target will be lower than the bombarding energy, and cross sections calculated using Eq. (5) will not reflect the true cross section, since the energy loss of the beam smears out the cross section, lowering and broadening the peaks of resonance structures. The deconvolution procedure we used to adjust the measured energies and cross sections for this effect applies a correction factor $f(\bar{E})$ to Eq. (5),

$$Y_n = (nt)f(\bar{E})\bar{\sigma}(\bar{E})\varepsilon(\bar{E}) , \tag{7}$$

where the energy $\bar{E}$ is no longer the beam energy, but is rather the average energy of the beam inside the target. An iterative procedure is used to calculate $\bar{E}$ and $f(\bar{E})$ from the formulas

$$\bar{E} = \frac{\int_{E_t}^{E} E'\sigma'(E')\varepsilon(E') \left[\frac{dE}{dX}(E')\right]^{-1} dE'}{\int_{E_t}^{E} \sigma'(E')\varepsilon(E') \left[\frac{dE}{dX}(E')\right]^{-1} dE'} \tag{8}$$

and

$$f = \frac{\int_{E_t}^{E} \sigma'(E')\varepsilon(E') \left[\frac{dE}{dX}(E')\right]^{-1} dE'}{\sigma'(\bar{E})\varepsilon(\bar{E}) \int_{E_t}^{E} \left[\frac{dE}{dX}(E')\right]^{-1} dE'} . \tag{9}$$

Initially $\sigma'(E')$ in these expressions is a fit to the $\sigma(E)$'s calculated using Eq. (5). Thereafter, $\bar{\sigma}(\bar{E})$, calculated using Eq. (7), is used to generate a new fit, and this process is repeated until the fit converges. Typically, the process took five iterations before the fit converged within associated errors.

The resulting cross sections, with scale uncertainty estimated to be 9%, are plotted in Fig. 5. The major contributions to the uncertainty are the error in the detector efficiency (8%), target thickness (3%), and target-thickness deconvolution procedure (3%). Statistical errors, current integration, and uncertainty in the incident beam energy made negligible contributions.

For $E_{\text{c.m.}} > 1.25$ MeV, our data agree with the Gibbons-Macklin cross sections [8] within uncertainty, but are on average 15% lower than the Geiger and Van der Zwan tabulation [19]. Below 1.25 MeV, although the Geiger and Van der Zwan tabulation falls off faster than our data, the two results still agree within uncertainty, while the Gibbons-Macklin data fall off still more rapidly.

If the resulting cross sections are convolved with the stopping powers from zero energy to E_α, the result is the thick-target yield per incident alpha particle,

$$Y_{\text{thick}} = \int_0^{E_\alpha} \sigma(E') \left[\frac{dE}{dX}(E')\right]^{-1} dE' , \tag{10}$$

corresponding experimentally to the yield in which a monoenergetic beam of energy E_α is completely stopped in the target. These yields are derived from experimental measurements by the formula

$$Y_{\text{measured}} = \bar{\varepsilon}\, Y_{\text{thick}} , \tag{11}$$

where $\bar{\varepsilon}$ is the effective efficiency, defined as

$$\bar{\varepsilon} = \frac{\int_0^{E_\alpha} \sigma'(E')\varepsilon(E') \left[\frac{dE}{dX}(E')\right]^{-1} dE'}{\int_0^{E_\alpha} \sigma'(E') \left[\frac{dE}{dX}(E')\right]^{-1} dE'} , \tag{12}$$

since the efficiency varies as the beam loses energy in

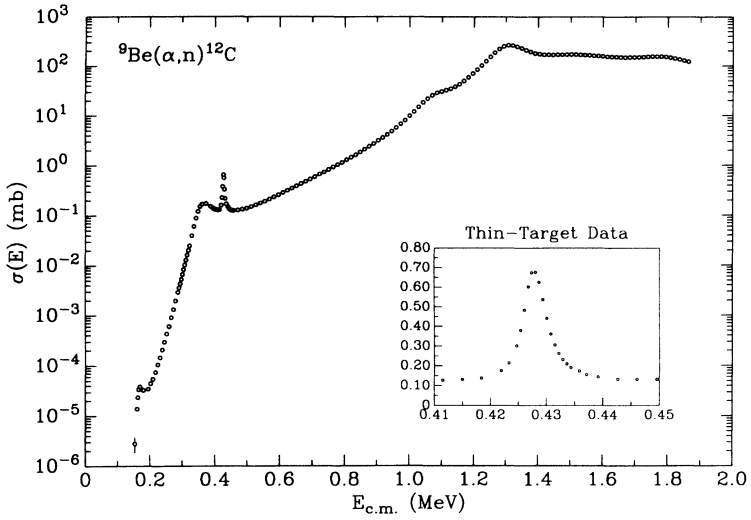

FIG. 5. Total cross sections for $^9\mathrm{Be}(\alpha,n)^{12}\mathrm{C}$ measured using the 18.4-μg/cm^2 target. The relative errors are smaller than the size of the data points. The normalization uncertainty of the data is estimated to be 9%. The inset shows the cross sections measured using the thin 0.76-μg/cm^2 target; these data were used for the S-factor fit to the narrow resonance.

the target. The $\sigma'(E')$ in this equation is the fit used in Eqs. (8) and (9).

The major contribution to the uncertainty in the yields is the 8% error in the neutron detector efficiency. When our measured thick-target yields, Fig. 6, were compared with the integration of our cross sections shown in Fig. 5, convolved with our stopping powers and efficiencies, for all but the lowest point the two results agreed within 3%, which is our uncertainty for the measured target thickness. Our thick-target yields agree well with the yields recently reported by Heaton *et al.* [12] for bombarding energies in the range $2.00 \leq E_\alpha \leq 2.30$ MeV, but are considerably higher for energies 1.60 and 1.80 MeV. As the Heaton values are derived by renormalizing an integration of the Gibbons-Macklin cross sections [8] with Ziegler's stopping powers, the discrepancy is likely due to the sharp dropoff of the Gibbons-Macklin cross sections below $E_{\mathrm{c.m.}} = 1.25$ MeV.

B. Astrophysical S factor

The astrophysical S factor, $S(E)$, is defined by

$$S(E) = \sigma(E) E \exp\left(\sqrt{\frac{E_G}{E}}\right) , \tag{13}$$

where E is the center-of-mass energy and E_G is the Gamow energy (173.6366 MeV [29] for $^9\mathrm{Be} + \alpha$). Our S factor for $^9\mathrm{Be}(\alpha,n)^{12}\mathrm{C}$ was fitted as a sum of Breit-Wigner peaks,

$$S(E) = \sum_{i=1}^{8} \frac{H_i \left(\frac{\Gamma_i}{2}\right)^2}{(E - E_i)^2 + \left(\frac{\Gamma_i}{2}\right)^2} , \tag{14}$$

with no background term required for a good fit. The maximum excursion of the fit from the data is 3% above

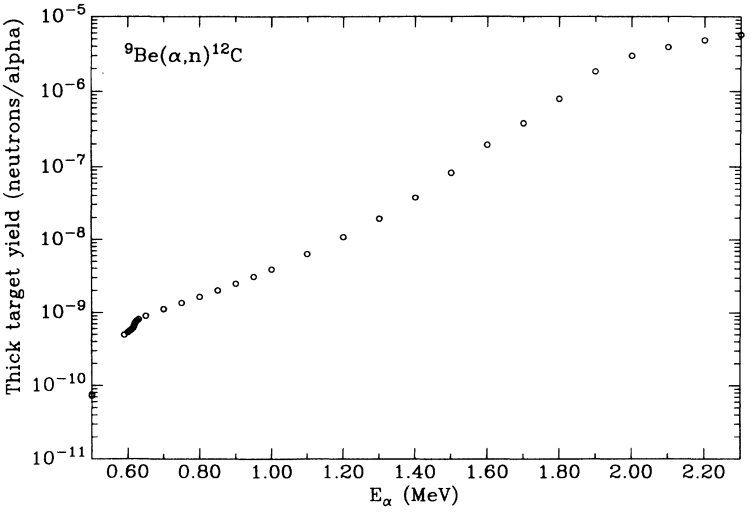

FIG. 6. Thick-target yields for $^9\mathrm{Be}(\alpha,n)^{12}\mathrm{C}$. Our data points have a scale uncertainty of 8%.

0.45 MeV, but in the valley near $E_{\text{c.m.}} = 0.25$ MeV, the excursion rises to 14%. Included in the fit is the resonance at 0.1062 MeV; the energy and width for this resonance were fixed at the values given by Cierjacks *et al.* [30], and the strength was derived from the relevant term in the Caughlan-Fowler rate [9]. The resonances at 0.166 and 0.428 MeV were fitted separately, the former because of the large statistical uncertainties in the low-energy data; the latter was fitted using the 0.76-μg/cm^2 target data. The S-factor data and fit are shown in Fig. 7, and the Breit-Wigner parameters are listed in Table I. The errors quoted for the fitting parameters are those associated with the fit and the counting statistics of the points, and do not include errors in the scale normalization of the data, the energy calibration, or the assumed form of $S(E)$.

Our values for the energies and widths of the resonances at 0.166 and 0.428 MeV agree with values derived from ^{12}C + n resonance parameters found by Cierjacks *et al.* [30]. Our value for the width of the 0.354-MeV resonance agrees with Davids [6], but our results for the energy of this resonance and the energy and width of the 0.428-MeV resonance disagree with the Davids values.

TABLE I. Parameters returned by fits of Eq. (14) to $S(E)$ for ^{9}Be$(\alpha, n)^{12}$C. The errors (errors in the least significant digits are shown in parentheses) quoted for the fitting parameters reflect the error associated with the fit, and do not include errors in the normalization of the data, energy calibration, or the assumed form of $S(E)$. Energies and widths are given in the center-of-mass frame.

E_i (MeV)	Γ_i (keV)	H_i (MeV b)
0.1062[a]	50.9[a]	3.395×10^{4}[b]
0.1663(3)	18.7(4)	$5.63(14) \times 10^{5}$
0.35403(4)	56.43(7)	$2.094(4) \times 10^{5}$
0.42787(1)	4.681(19)	$1.388(5) \times 10^{5}$
1.0776(3)	122.5(8)	$4.683(19) \times 10^{3}$
1.2974(1)	148.7(4)	$2.987(6) \times 10^{4}$
1.4929(8)	370.2(17)	$7.77(3) \times 10^{3}$
1.7714(6)	226(3)	$2.23(2) \times 10^{3}$

[a]From Ref. [30].
[b]From Ref. [9].

C. Reaction rates

The thermonuclear reaction rate $N_A\langle\sigma v\rangle$ for non-identical particles is given by [31]

$$N_A\langle\sigma v\rangle = \left[\frac{8}{\mu\pi}\right]^{\frac{1}{2}} \frac{N_A}{(kT)^{\frac{3}{2}}} \int_0^\infty \sigma(E) E \exp\left[-\frac{E}{kT}\right] dE \,, \tag{15}$$

where N_A is Avogadro's number, μ is the reduced mass in the entrance channel, k is Boltzmann's constant, T is the temperature, and E is the energy in center of mass. The integration was performed numerically, using our S-factor parameters given in Table I for $0.00 \leq E_{\text{c.m.}} \leq 1.87$ MeV, and using the Gibbons-Macklin cross sections [8] for $1.87 \leq E_{\text{c.m.}} \leq 7.50$ MeV. Below the range of our data, $E_{\text{c.m.}} < 0.16$ MeV, the S factor was assumed to be due entirely to the 0.1062 MeV resonance and the tails from higher resonances; this region contributes $\approx 6.5\%$ to the calculated reaction rate at $T = 0.1$ GK. Above 7.50 MeV, the cross section was assumed to be constant, 800 mb, contributing 0.9% to the rate at $T = 10$ GK. The reaction rates resulting from this integration, plotted in Fig. 8, were fitted to within 2% for $0.1 \leq T \leq 10$ GK by the analytical expression

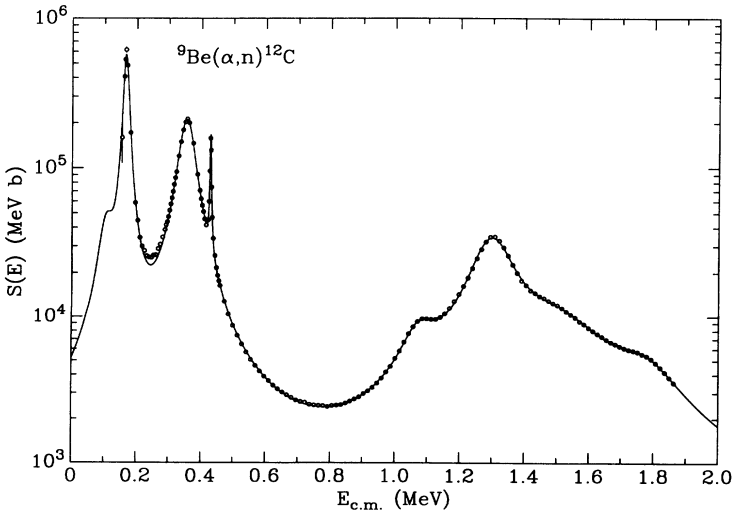

FIG. 7. The S factor for ^{9}Be$(\alpha, n)^{12}$C, calculated from the data of Fig. 5. The solid curve is the fit to Eq. (14), with parameters as described in Table I.

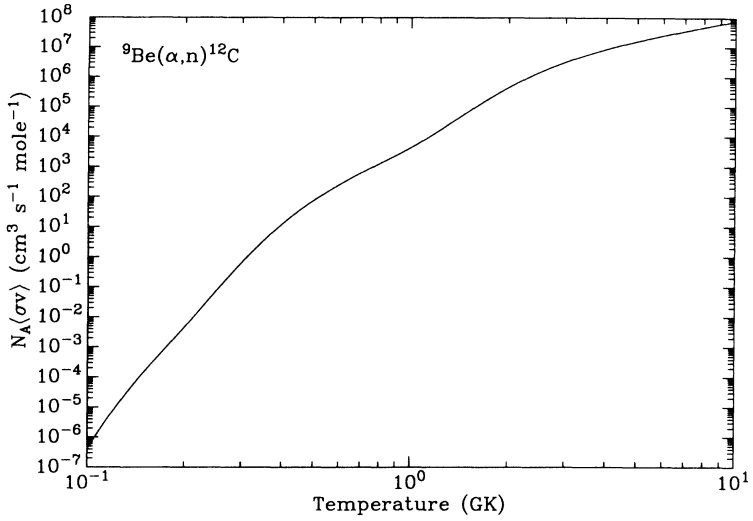

FIG. 8. The thermonuclear reaction rate $N_A\langle\sigma v\rangle$ for $^9\mathrm{Be}(\alpha,n)^{12}\mathrm{C}$ calculated from our data and extrapolation as described in the text. Equation (16) is an analytical approximation (±2%) for this rate.

$$
\begin{aligned}
N_A\langle\sigma v\rangle = {} & 6.476\times10^{13}\quad T^{-2/3}\exp\left(-\frac{23.8702}{T^{1/3}}\right)\times\left(1.0-0.3270T^{1/3}\right)+6.044\times10^{-3}\quad T^{-3/2}\exp\left(-\frac{1.401}{T}\right)\\
& +7.268\times10^{0}\quad T^{-3/2}\exp\left(-\frac{2.063}{T}\right)+3.256\times10^{4}\quad T^{-3/2}\exp\left(-\frac{3.873}{T}\right)\\
& +1.946\times10^{5}\quad T^{-3/2}\exp\left(-\frac{4.966}{T}\right)+1.838\times10^{9}\quad T^{-3/2}\exp\left(-\frac{15.39}{T}\right), \qquad (16)
\end{aligned}
$$

where T is the temperature in GK. This analytical expression then has an overall uncertainty of 10%, including the normalization uncertainty in the cross sections. The first term in the rate is the expression for the rate due to a slowly varying S factor, with the leading term and the coefficient in the polynomial allowed to vary in the fit. The remaining terms are the contributions for the rate from the resonances at 0.1062, 0.166, 0.354, 0.428, and 1.297 MeV, respectively. Since all but the third resonance are broad ($\Gamma > 0.1E_R$), the factors in the exponents of these terms were also allowed to vary. All other resonance contributions are included in the first term.

Figure 9 compares our expression for the reaction rate, Eq. (16), with the rate given by Caughlan and Fowler [9]. Our rate is a factor of 7 higher than the Caughlan-Fowler rate near $T = 0.15$ GK. Above $T = 0.2$ GK, the maximum excursion in the ratio is about 1.65, near 1 GK.

The reaction rate includes a small contribution from the reaction $^9\mathrm{Be} + \alpha \rightarrow 3\alpha + n$, as this reaction is kinematically allowed for center-of-mass energies above 1.6 MeV. However, Geiger and Van der Zwan [19] found that the breakup cross section is appreciable only for energies above 3.0 MeV, so the breakup contribution to the reaction rate is less than 5% for $T < 7$ GK.

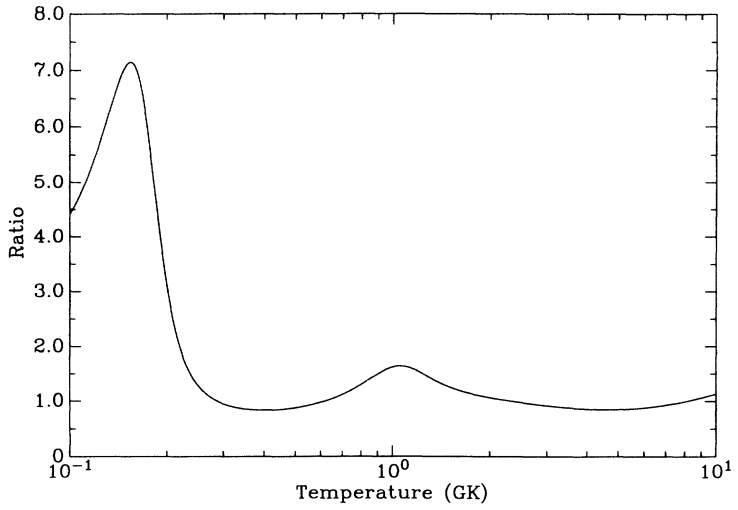

FIG. 9. Comparison of our reaction rate with the Caughlan-Fowler rate [9]. The ratio shown is our analytical expression divided by the Caughlan-Fowler expression.

IV. CONCLUSIONS

The $^9\mathrm{Be}(\alpha,n)^{12}\mathrm{C}$ cross sections have been measured for $0.16 \leq E_{\mathrm{c.m.}} \leq 1.87$ MeV, and agree with the Gibbons-Macklin cross sections [8] for $E_{\mathrm{c.m.}} > 1.25$ MeV. Thermonuclear reaction rates have been calculated by numerical integration of these cross sections to a precision of $\pm 10\%$ for $0.1 \leq T \leq 10$ GK; these rates differ by up to $\approx 65\%$ with the previously tabulated rates [9] above $T = 0.2$ GK, and are a factor of 7 higher near $T = 0.15$ GK. These new rates, with uncertainty much smaller than the previous factor of 3, provide a greatly improved basis for explosive nucleosynthesis calculations.

This work was supported in part by the National Science Foundation Grant No. PHY91-15574.

[1] C. W. Cook, W. A. Fowler, C. C. Lauritsen, and T. Lauritsen, Phys. Rev. **107**, 508 (1957). This reference has an interesting summary of the early work establishing crucial properties of the resonant 3α reaction.
[2] M. D. Delano and A. G. W. Cameron, Astrophys. Space Sci. **10**, 203 (1971).
[3] S. E. Woosley and R. D. Hoffman, Astrophys. J. **395**, 202 (1992).
[4] G. Kuechler, A. Richter, and W. von Witsch, Z. Phys. A **326**, 447 (1987).
[5] F. Ajzenberg-Selove, Nucl. Phys. **A490**, 1 (1988).
[6] C. N. Davids, Ph.D. thesis, California Institute of Technology, 1967; Nucl. Phys. **A110**, 619 (1968); Astrophys. J. **151**, 775 (1968).
[7] L. Van der Zwan and K. W. Geiger, Nucl. Phys. **A152**, 481 (1970).
[8] J. H. Gibbons and R. L. Macklin, Phys. Rev. **137**, B1508 (1965).
[9] G. R. Caughlan and W. A. Fowler, At. Data Nucl. Data Tables **40**, 283 (1988).
[10] W. A. Fowler, cited in Ref. [3].
[11] J. F. Ziegler, *The Stopping and Ranges of Ions in Matter* (Pergamon, New York, 1977), Vols. 3 and 4.
[12] R. Heaton, H. Lee, P. Skensved, and B. C. Robertson, Nucl. Instrum. Methods A **276**, 529 (1989).
[13] A. H. Wapstra and G. Audi, Nucl. Phys. **A432**, 1 (1985).
[14] F. Ajzenberg-Selove, Nucl. Phys. **A475**, 1 (1987). It should be noted that the quoted Q_m value of (-2.4387) for the $^{18}\mathrm{O}(p,n)^{18}\mathrm{F}$ neutron threshold in this tabulation should actually read (-2.4377) to agree with both the values in Table I of the same reference and the atomic masses given by Wapstra [13].
[15] C. R. Brune and R. W. Kavanagh, Phys. Rev. C **44**, 1665 (1991).
[16] T. R. Wang, R. B. Vogelaar, and R. W. Kavanagh, Phys. Rev. C **43**, 883 (1991).
[17] J. W. Maas, A. J. C. D. Holvast, A. Baghus, H. J. M. Aarts, and P. M. Endt, Nucl. Phys. **A301**, 213 (1978).
[18] C. R. Brune, R. W. Kavanagh, S. E. Kellogg, and T. R. Wang, Phys. Rev. C **43**, 875 (1991).
[19] K. W. Geiger and L. Van der Zwan, Nucl. Instrum. Methods **131**, 315 (1975).
[20] R. K. Bardin, Ph.D. thesis, California Institute of Technology, 1961.
[21] V. Ya. Golovnya, A. P. Klyucharev, B. A. Shilyaev, and N. A. Shlyakhov, Yad. Fiz. **4**, 770 (1967) [Sov. J. Nucl. Phys. **4**, 547 (1967)].
[22] H. H. Andersen, C.C. Hanke, H. Sørensen, and P. Vajda, Phys. Rev. **153**, 338 (1967).
[23] F. S. Mozer, Phys. Rev. **104**, 1386 (1956).
[24] Á. Kiss, E. Koltay, Gy. Szabó, and L. Végh, Nucl. Phys. **A282**, 44 (1977). We interpolated between two of their measurements to get a value for $\theta_{\mathrm{lab}} = 142.4°$.
[25] R. A. Langley, M. Lewis, and R. A. Zuhr, Nucl. Instrum. Methods B **29**, 599 (1988).
[26] W. K. Chu and D. Powers, Phys. Rev. **187**, 478 (1969).
[27] F. Hinterberger, R. Schönhagen, P. von Rossen, B. Schüller, F. E. Blumenberg, P. D. Eversheim, and R. Görgen, Nucl. Phys. **A308**, 61 (1978).
[28] J. H. Gibbons and R. L. Macklin, Phys. Rev. **114**, 571 (1959).
[29] The nuclear masses (in amu) were derived from Ref. [13], and the atomic mass constant, 931.494 32(28) MeV/c^2, was taken from Particle Data Group, Phys. Rev. D **45**, S1 (1992).
[30] S. Cierjacks, F. Hinterberger, G. Schmalz, D. Erbe, P. v. Rossen, and B. Leugers, Nucl. Instrum. Methods **169**, 185 (1980).
[31] W. A. Fowler, G. R. Caughlan, and B. A. Zimmerman, Annu. Rev. Astron. Astrophys. **5**, 525 (1967).